Phonon dispersion relation of metallic glasses

Daniel Crespo,[1,*] Pere Bruna,[1] Araceli Valles,[2] and Eloi Pineda[1]
[1]*Departament de Física, Universitat Politécnica de Catalunya, BarcelonaTech, 08860-Castelldefels, Catalonia, Spain*
[2]*Aviation & Marine, Qatar RE, Bleicherweg 72, Zurich, Switzerland*
(Received 24 October 2015; revised manuscript received 14 August 2016; published 13 October 2016)

Experimental data on the phase sound speed of metallic glasses show anomalies in the terahertz range, reflecting an underlying complex behavior of their phonon dispersion spectrum not yet explained. We determine the phonon dispersion curve of metallic glasses by means of massive molecular dynamics simulations, allowing us to obtain the low-q region behavior with unprecedented detail. Results confirm that the sound speed is constant below the THz range, down to the macroscopic limit. On the contrary, a hardening of the sound speed, more notable in the transverse case, is found in the THz range. This behavior is modeled in terms of a relaxation model. The model gives quantitative agreement and allows us to determine a new threshold frequency ω_h, at the end of the boson-peak region. Above ω_h the shear modulus increases dramatically, reflecting the end of the amorphous-like acoustic propagation region characterized by the excess density of vibrational states.

DOI: 10.1103/PhysRevB.94.144205

I. INTRODUCTION

The phonon spectrum reflects the mechanical properties of a material at the atomic level. In the case of metallic glasses (MGs), from the atomic perspective [1] their mechanical properties can only be described from a statistical point of view. Accordingly, the phonon spectrum of MGs gives a privileged gauge of the interplay between cohesive atomic forces and glass topology [2].

The access to the phonon spectrum of metallic glasses is limited by experimental constraints. The main available experimental technique, inelastic x-ray scattering (IXS), allows one to test most of the pseudo-Brillouin zone but cannot access the low-wave-number q region. Thus, there is a gap at the mesoscopic scale, between the ultrasound range accessible macroscopically and the terahertz range accessible by IXS. In addition, experimental data of phonon dispersion and damping is restricted to the longitudinal modes, while the effects of the amorphous structure are expected to be more significant in the transverse polarizations. Furthermore, IXS measurements in MG offered contradictory results. Ichitsubo *et al.* [3] reported a hardening on the sound speed, i.e., at low q the phase velocity increases with increasing frequency, and proposed a model for fragile metallic glasses in which nanometric islands of strongly bonded regions are surrounded by a skeleton of weakly bonded regions. This model predicts a positive deviation from the linear behavior in the phonon dispersion relation at q around the inverse of the size of the strongly bonded regions. That means that the sound velocity of nanometer-order wavelength should be higher than the corresponding millimeter-order wavelength. However, later IXS experiments were not conclusive [4,5] or even contradictory [6].

Theoretical models and experimental results in other types of glasses have also predicted transitions between different regimes of phonon dispersion and damping at the nanometer-scale. Schober [7] stressed the importance of quasilocalized vibrations (QLV) in the phonon spectrum of glasses. The coupling of QLV would be the origin of the boson peak (BP), and thus the high-wave-number regime would display hybridization between phonons and QLV. In this model the positive dispersion, i.e., the change from "soft" (lower speed) to "hard" (higher speed) phonon propagation, is observed at the frequency corresponding to the BP maximum. The model predicts also a change in the increase of the broadening of the phonon branch from a $\propto\omega^4$ to a lower power law with exponent depending on the parameter values used in the model. A transition of the damping behavior from $\propto q^4$ to $\propto q^2$ was observed in densified SiO_2, in this case attributed to a change from amorphous to crystal-like vibrational dynamics [8]. Positive deviation of the phonon dispersion was also observed in disordered systems like liquids where it has been explained using the mode coupling theory [9].

Molecular dynamics (MD) simulations may help to fill the gap, but low wave numbers are only accessible in very large boxes. Furthermore, most of the available results were obtained by using Lennard-Jones (LJ) or soft-sphere (SS) potentials [10–12]. Marruzzo *et al.* [12] simulated a binary mixture of 10^7 particles with a SS potential and showed that the spatial fluctuations of the elastic constants on a microscopic length scale are responsible for the BP and the other elastic anomalies in the high frequency vibrational dynamics of glasses. In agreement with experimental [13] and numerical [10] results, a negative dispersion of the sound velocity and a steep increase ($\propto \omega^4$) in the width of the excitation in the BP region was detected. Later, Mizuno *et al.* [14,15] used a model with SS interatomic interactions in which they can introduce several degrees of disorder and, thus, study within the same framework a fully crystalline structure and a fully amorphous one. They computed the sound velocities and, as in previous works, they found a softening of the transverse sound velocity. Furthermore, they computed the bulk and shear moduli from the sound velocity data and they found that the bulk modulus is constant and equal to the macroscopic value below the BP frequency but decreases at higher frequencies. Therefore, this result is at odds with the assumption of a frequency-independent bulk modulus proposed in Refs. [10,12]. Mizuno *et al.* argue that the details of the interaction potential can play a nontrivial role and cause this discrepancy. The importance of these details is also pointed out

*Daniel.Crespo@upc.edu; http://mie.esab.upc.es/mmn

by Monaco *et al.* [10], who question what role anharmonicity plays in glasses, as the LJ potential of monoatomic glasses has been proven to be well described within the framework of the harmonic approximation [16]. As real glasses are anharmonic systems, the question that immediately arises is whether the LJ or the SS potentials are the proper potentials to study the dynamics of real glasses. And the contradiction remains, as until now no numerical simulation predicts the hardening of the sound speed observed experimentally.

Liquid dynamics at low particle densities (high temperatures) scales with density and temperature, showing a universal behavior weakly dependent on the particular type of interatomic potential and totally independent of the long-range attractive potential tail [17]. This density scaling dynamics is indeed observed between systems sharing the same type of bonding in different families of glass formers. Contrarily, Berthier *et al.* [18] showed that this universal density scaling is violated in the dense supercooled liquid and glassy regimes. There, the long-range details of the potential, like anharmonicity, have important effects on the dynamics of the system. The topological structure of glasses is dominated by the maximization of atomic packing and, therefore, the long-range interaction has small influence on it, but the details of the potential tail deeply affect the mechanical heterogeneity of glasses and, accordingly, their vibrational behavior [19]. The mesoscale mechanical heterogeneity (soft-stiff fluctuations) widely observed in simulations [20] and already detected experimentally in metallic glasses [21] is then expected to be highly dependent on the details of the particular interatomic potential of the system.

Here we report massive molecular dynamics simulations of metallic glasses dynamics using the embedded atom method. As the details of the potential are expected to have a major influence in the expected results, the simulations are compared to those of crystalline materials of similar compositions. Hardening of the sound speed is observed in the analyzed compositions, and a model accounting for its origin is presented.

II. MOLECULAR DYNAMICS SIMULATIONS

Simulations of two amorphous systems, namely $Zr_{50}Cu_{40}Al_{10}$ and $Pd_{82}Si_{18}$, and a crystalline system, ZrCuAl, were performed. The embedded atom method (EAM), originally developed by Daw and Baskes [22], is a many-body potential where the total energy is given by

$$E = \frac{1}{2}\sum_{i,j,i\neq j}\phi_{ij}(r_{ij}) + \sum_{i}F_i(\rho_i),$$

where ϕ_{ij} represents the pair energy between atoms i and j separated by a distance r_{ij}, and F_i is the embedding energy associated with an atom i placed into a local site with electron density ρ_i. The electron density is calculated using

$$\rho_i = \sum_{j,j\neq i} f_j(r_{ij}),$$

where f_j is the contribution to the electron charge density from atom j at the location of atom i. In order to describe the interaction between the elements in the alloy, the pair energy

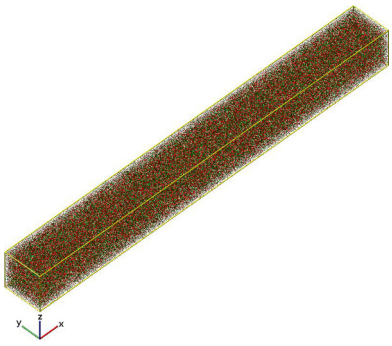

FIG. 1. Box geometry.

ϕ_{ab} between each possible pair must be supplied in addition to the electron density ρ and the embedding energy F for each of the elements. EAM has been successfully used in the study of metallic glasses, though it has been shown that specific potentials must be used to obtain reliable results in the amorphous state. Here we use the potentials developed for the glass state by Cheng [23] and Sheng [24] specifically for amorphous ZrCuAl and PdSi metallic glasses, respectively.

Simulations were performed on cubic and high-aspect-ratio rectangular boxes of dimensions $l_x : l_y : l_z$ with $l_x \gg l_y = l_z$. In this way, the wave numbers accessible on the x direction (long edge) are much lower than in the y and z directions (short edges), allowing us to explore the phonon dispersion and damping in the low-wave-number region without an excessive increase in the number of simulated atoms. Figure 1 shows the geometry of a 10:1:1 box.

The Large-scale Atomic/Molecular Massively Parallel Simulator (LAMMPS) code [25] was used, with a time step of 0.001 ps and periodic boundary conditions. The parameters of the simulated systems are given in Table I. In the glassy systems the liquid was equilibrated in the isothermal-isobaric (NPT) ensemble at 2000 K for 2 ns, and then it was quenched at the desired quenching rate down to 300 K. The glasses were subsequently equilibrated during 2 ns in NPT conditions before computing the static and dynamic structure factors, which were computed in the canonical (NVT) ensemble for 1 ns. The values obtained along different directions and boxes are in excellent agreement, indicating that the box shape is not influencing the phonon dynamics.

TABLE I. Parameters of the simulated systems.

Box size (Å^3)	Atoms	Quenching rate (K s^{-1})
	$Pd_{82}Si_{18}$ glass	
$\sim 80 \times 80 \times 80$,	3.2×10^4	10^{13}, 10^{12}
$\sim 800 \times 80 \times 80$,	3.2×10^5	10^{13}, 10^{12}
$\sim 8000 \times 80 \times 80$,	3.2×10^6	10^{13}
	$Zr_{50}Cu_{40}Al_{10}$ glass	
$\sim 80 \times 80 \times 80$,	3.2×10^4	10^{13}, 10^{12}, 10^{10}
$\sim 800 \times 80 \times 80$,	3.2×10^5	10^{13}, 10^{12}
	ZrCuAl crystalline	
$\sim 800 \times 80 \times 80$,	3.2×10^4	–

The density of states $g(\omega)$ was computed as the Fourier transform of the velocity self-correlation function, defined as

$$C_v(t) = \langle \vec{v}_i(0) \cdot \vec{v}_i(t) \rangle. \quad (1)$$

The static structure factor $S(q)$ was computed as the Fourier transform of the pair distribution function $g(r)$:

$$g(r) = \frac{1}{N} \sum_{i \neq j} \langle \delta(r - |\vec{r}_i - \vec{r}_j|) \rangle. \quad (2)$$

The dynamic structure factor was computed as the self-correlation of the particle current functions $j_\alpha(\vec{q},t)$,

$$S_\alpha(\vec{q},\omega) = \frac{\vec{q} \cdot \vec{q}}{2\pi\omega^2 N} \int dt \langle j_\alpha(\vec{q},t) \cdot j_\alpha(-\vec{q},0) \rangle e^{I\omega t}, \quad (3)$$

where $\alpha = L,T$ stands for longitudinal and transverse excitations, respectively, $\vec{q}$ is the wave vector, ω is the excitation frequency, N is the number of particles, and

$$\begin{aligned} j_L(\vec{q},t) &= \sum [\vec{v}_i(t) \cdot \hat{q}] \hat{q} e^{I\vec{q}\cdot\vec{r}_i(t)} \\ j_T(\vec{q},t) &= \sum [\vec{v}_i(t) - (\vec{v}_i(t) \cdot \hat{q})\hat{q}] e^{I\vec{q}\cdot\vec{r}_i(t)}, \end{aligned} \quad (4)$$

$\vec{r}_i(t)$ and $\vec{v}_i(t)$ being the position and velocity of particle i at time t, respectively.

In order to study the dispersion curve and the damping of the acoustic waves the dynamic structure factor $S_\alpha(\vec{q},\omega)$, computed for each wave number $\vec{q}$ as a function of the frequency ω, was fitted to a damped harmonic oscillator response [26],

$$I \propto \frac{\omega^2 \Gamma_q}{\left[\Omega_q^2 - \omega^2\right]^2 + \omega^2 \Gamma_q^2}, \quad (5)$$

where Ω_q is the eigenfrequency and Γ_q accounts for the broadening of the phonon excitations at wave vectors of modulus q.

III. RESULTS

Figure 2 shows the static structure factor of the simulated glasses. Despite the very different compositions, $S(q)$ shows very similar features in the two glasses. The effect of the quenching rate in the amorphous structure is almost not perceived in both cases.

Figure 3 shows a typical example of $S_L(\vec{q},\omega)$ in the studied MGs. While $S_L(\vec{q},\omega)$ is single peaked in $Zr_{50}Cu_{40}Al_{10}$, it shows a secondary resonance in $Pd_{82}Si_{18}$ at higher frequencies. $S_T(\vec{q},\omega)$ shows the same behavior. To understand the origin of this second resonance, $S_L(\vec{q},\omega)$ is plotted for two values of q in this case. The low-frequency resonance behaves as the expected acoustic branch; the resonance frequency increases with the wave number and its intensity decreases as q increases. On the contrary, the high-frequency resonance has an almost constant shape, independent of q. Its low intensity makes it difficult to detect at low q although it is always present. The partial dynamic structure factors, also shown in the figure, show that only Si atoms contribute to the high-frequency resonance. This indicates that rather than an optical phonon branch, this resonance is associated to Einstein oscillators created by a sort of caging effect of the Si atoms. Note that the corresponding Einstein temperature

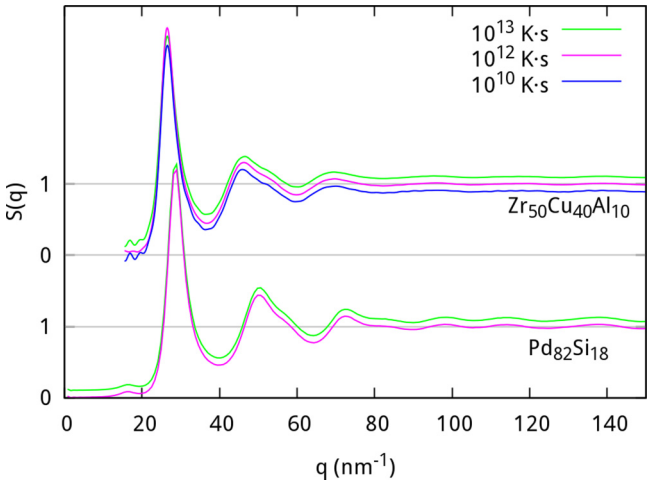

FIG. 2. Static structure factor $S(q)$ of the simulated glasses, quenched at different quenching rates. $S(q)$ of the same glass quenched at different quenching rates are shifted vertically to allow comparison.

is about 550 K, while the glass is being simulated at 300 K. Einstein oscillators were already reported in MGs [27] but with much lower energies. In these cases, they were associated to phonon localized modes, while here they seem to correspond to individual atomic movements. However, Hosokawa reported recently unexpected vibrational modes in $Pd_{40}Ni_{40}P_{20}$ in the same range of energies [28], which may have a similar origin. This effect is most probably due to the large mass difference between Pd and Si, as $m_{Pd}/m_{Si} \sim 3.8$.

Figure 4 shows the phase sound speeds c_L (longitudinal) and c_T (transverse) computed in $Pd_{82}Si_{18}$ and $Zr_{50}Cu_{40}Al_{10}$ vitrified at a quenching rate (QR) of 10^{12} K s^{-1}. Similar plots for the remaining quenching rates are given in the supplemental material [29]. Both c_L and c_T show a constant value in the macroscopic limit, as shown in the figure inset. This is the only possible physically meaningful result; otherwise,

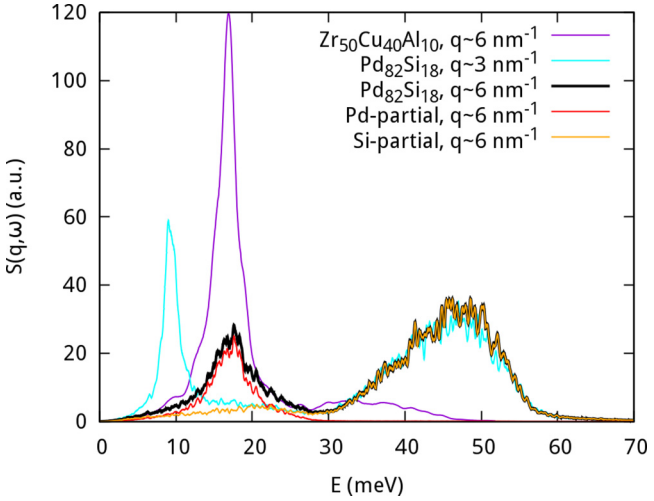

FIG. 3. Dynamic structure factor $S(\vec{q},\omega)$ of the studied MG quenched at 10^{12} K s^{-1} for two particular values of q, and partial structure factors of Pd and Si in $Pd_{82}Si_{18}$ at $q \sim 6$ nm^{-1} (see text).

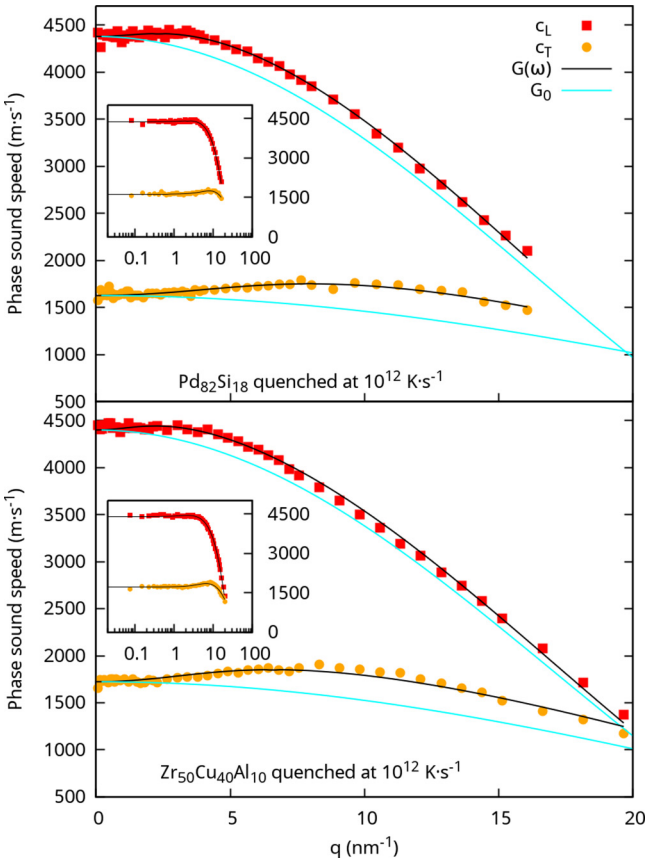

FIG. 4. Longitudinal (c_L) and transverse (c_T) phase sound speeds of the simulated glasses in linear and semilogarithmic scale (inset) to show the behavior in the $q \to 0$ (macroscopic) limit. Solid lines correspond to the model developed in Sec. IV.

the macroscopic sound speed should show some kind of anomaly. At increasing wave numbers, $q > 1$ nm^{-1}, a hardening on both speeds is noticed. The maximum on the hardening appears at larger wave numbers for transverse than for longitudinal excitations. This fact contrast with pseudopotential simulations of MG [30,31] and in monoatomic LJ glasses [10], where a direct correlation between the longitudinal and transverse sound speed was found by assuming a frequency independent bulk modulus.

Figure 5 shows the frequency dependence of sound attenuation coefficients for longitudinal and transverse excitations. The broadening of the transverse acoustic excitation shows a linear dependence on ω at high frequencies, while it changes to a quadratic dependence when approaching the macroscopic limit ($\omega \to 0$), as expected for propagating waves in an amorphous homogeneous media. Similar dependencies are expected in longitudinal excitations, but they are not clear in $Pd_{82}Si_{18}$. This is probably due to the effect of the above-cited Einstein oscillators, which affect the high-frequency behavior of the acoustic excitations. It is worth mentioning that, due to the small size of the box, the data for the quenching rate of 10^{10} K s^{-1} do not allow us to determine the ω^2/ω crossover in this case. It has been largely discussed that the dependence should change again to ω^4 at very low ω due to Rayleigh scattering, as found in LJ glasses [10] and other glasses like glycerol and some network glasses [32]. In our case, the dispersion on the data increases noticeably below 3 THz in longitudinal excitations and may admit an ω^4 dependence, but at very low frequencies this behavior is lost. This dispersion is due to the very long simulation times needed to compute the eigenfrequencies corresponding to very low wave numbers and does not allows us to confirm or discard the ω^4 dependence. In the case of transverse excitations, the characteristic frequencies are always lower than for longitudinal excitations, and the required simulation times are even longer. Accordingly, the dispersion of the data that may correspond to an ω^4 dependence appears at lower frequencies than for longitudinal excitations.

Figure 6 shows the reduced density of states (DOS) of the simulated glasses. The intensity of the boson peak is

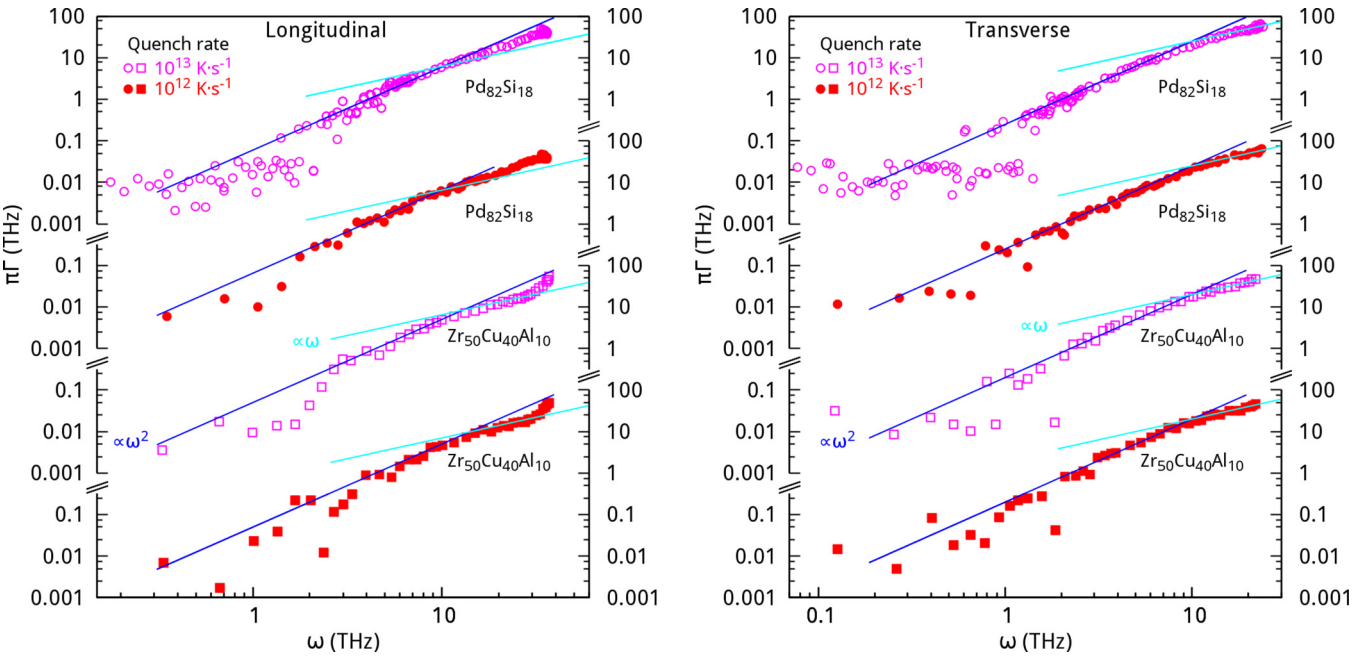

FIG. 5. Phonon disperson plots of longitudinal (left) and transverse (right) excitations.

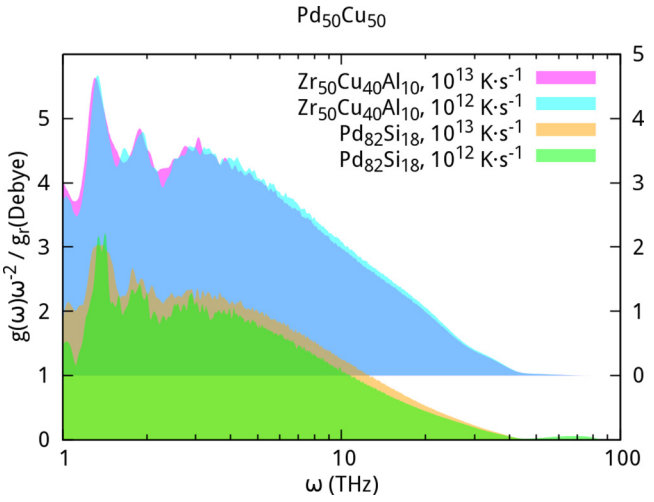

FIG. 6. Reduced density of states of the simulated glasses showing the intensity of the boson peak in each case.

very similar in $Zr_{50}Cu_{40}Al_{10}$ regardless the quenching rate and decreases very slightly in $Pd_{82}Si_{18}$ as the quenching rate decreases. A decrease of the excess density of states is expected in more stable glasses and it is closely related to a change in the shear modulus [33]. In this sense, the slight decrease in the DOS of $Pd_{82}Si_{18}$ is consequent with the small increase of shear modulus detected in this case.

The two most salient features of the dispersion relation are that there is no signature of softening in the low-q region, in fact, the $c_{L,T}(q \to 0)$ behavior is strikingly flat, and that the hardening transition appears at different wavelengths for longitudinal and transverse polarizations. However, when plotted as a function of frequency (Fig. 7), for $Pd_{82}Si_{18}$, the behavior of both phase sound speeds shows a common trend: Both increase up to a frequency ∼16 THz (a hardening effect) and then drop. This decrease is related to the bending of

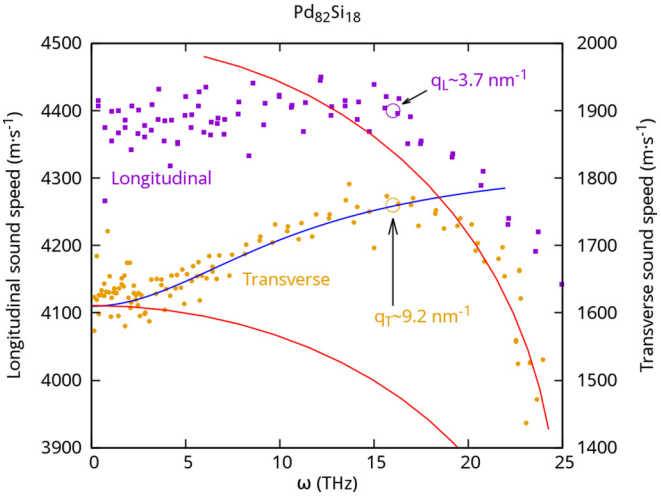

FIG. 7. Phase sound speed of $Pd_{82}Si_{18}$ quenched at 10^{12} K s^{-1} vs. frequency. The red solid lines show the behavior of two simple sinusoidal dispersion relations for the transverse sound speed obtained with different values of the shear modulus. The blue line shows the behavior of a viscoelastic-like transition.

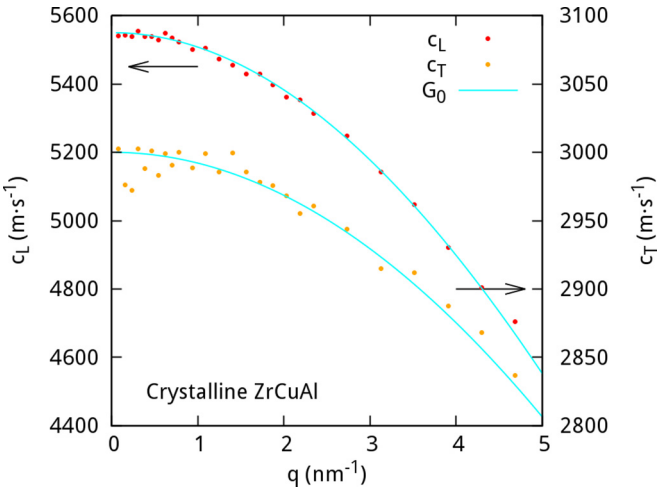

FIG. 8. Phase sound speeds computed in crystalline ZrCuAl at 300 K. Solid lines show the fit to simple sinusoidal relations of dispersion for the longitudinal and transverse excitations.

the dispersion curve when approaching the pseudo-Brillouin zone boundary, at ≈15 nm^{-1}. Note that the Debye frequency $\omega_D \sim 23$ THz in both glasses. Remarkably, the values of the wave numbers at which the sound speeds show their maxima, indicated in Fig. 7, differ considerably for longitudinal and transverse excitations. These facts suggest that the anomalies in the phase sound speed are due to a frequency effect rather than to any spatial feature.

It order to ensure that these results are actual features of the glass dynamics, not due to the EAM potential used in the simulations, crystalline ZrCuAl ($Fd\bar{3}m$ space group) was also simulated at 300 K using the same potential. Figure 8 shows the longitudinal and transverse phase sound speeds in this case, plotted up to 5 nm^{-1}; above this wavelength the acoustic and optic branches merge and it is not possible to determine precisely the sound speed. Both sound speeds are much higher than in the $Zr_{50}Cu_{40}Al_{10}$ glass; in particular, the transverse sound speed is almost doubled. Furthermore, both sound speeds are well fitted to simple sinusoidal relations of dispersion such as

$$\omega_{L,T}(q) = A_{L,T} \sin\left(\frac{qa}{2}\right), \tag{6}$$

where L and T stand for longitudinal and transverse, $\omega_{L,T}(q)$ are the eigenfrequencies of L and T excitations with wave vector q, and a is the lattice parameter. Thus, the crystalline structure shows no signs of hardening, and an explanation for the anomalies observed should be related to the glass structure.

IV. MODEL OF THE DISPERSON RELATION

Phonon dispersion curves in binary metallic glasses were computed by using pseudopotential methods [30,34], obtaining simple dispersion relations close to the classical sinusoidal form

$$\omega_{L,T}(q) = A_{L,T} \sin\left(\frac{\pi q}{Q_{L,T}}\right), \tag{7}$$

where Q_L is somewhat less than the position of the first diffraction peak (i.e., the wave vector at the boundary of the pseudo-Brillouin zone) and $Q_T > Q_L$. The longitudinal and transverse amplitudes are given by

$$A_L = \frac{Q_L}{\pi}\sqrt{\frac{K+\frac{4}{3}G}{\rho}}, \qquad A_T = \frac{Q_T}{\pi}\sqrt{\frac{G}{\rho}}, \tag{8}$$

K and G being the bulk and shear modulus and ρ the density of the material. However, these computations did not predict any hardening of the phase sound speed.

The red lines in Fig. 7 show the expected behavior of simple sinusoidal relations of dispersion corresponding to two values of the shear modulus G. The lower one is drawn for the value of G corresponding to the macroscopic value of c_T; we will call it *soft*. The discrepancy with the simulated data is striking. On the contrary, the high-frequency region is well fitted by a simple sinusoidal relation of dispersion computed for a much higher value of the shear modulus than for $q \to 0$; this will be referred to as *hard*. In order to model the transition from *soft* to *hard* dispersion relations, we propose a simple Maxwell model of a viscoelastic transition. In the Maxwell model the bulk and shear modulus depend on the frequency,

$$\begin{aligned} K(\omega) &= K_0 + (K_\infty - K_0)\frac{\omega^2\tau^2}{1+\omega^2\tau^2}, \\ G(\omega) &= G_0 + (G_\infty - G_0)\frac{\omega^2\tau^2}{1+\omega^2\tau^2}, \end{aligned} \tag{9}$$

where $K_{0,\infty}$ and $G_{0,\infty}$ are the bulk and shear modulus at macroscopic ($\omega \to 0$) and infinite frequencies, respectively. The blue line in Fig. 7 is a qualitative fit of such a viscoelastic transition to the low-frequency region of the transverse phase sound speed. The parameter τ corresponds to the characteristic relaxation time of the Maxwell model, and it allows us to define a corresponding threshold frequency $\omega_h = \tau^{-1}$.

The resulting relations of dispersion can be solved analytically. The phase speed of longitudinal and transverse oscillations is then

$$c_{L,T}(q_{L,T}) = \frac{\omega_{L,T}(q_{L,T})}{q_{L,T}}. \tag{10}$$

The dark solid lines in Fig. 4 show the fit of c_L and c_T by using Eqs. (7)–(9). The fit was performed simultaneously on both speeds, the fitting parameters being $K_{0,\infty}$, $G_{0,\infty}$, $Q_{L,T}$, and τ. Table II shows the results of the fits. The fitted value of Q_L for all materials and quenching rates is somewhat lower than Q_{Lexp}, the q value of the first peak of the static structure factor $S(q)$ shown in Fig. 2, as expected. The magnitude of the hardening due to the frequency-dependent elastic modulus is noted by comparison with the expected phase speed obtained without the frequency correction (cyan solid line in Fig. 4). While the bulk modulus remains constant at all frequencies, the shear modulus increases in the infinite frequency limit by 50% in $Zr_{50}Cu_{40}Al_{10}$ and is more than doubled in $Pd_{82}Si_{18}$. This fact explains why the effect is pronounced in the transverse phase sound speed, while it is much more subtle in the longitudinal sound speed. The frequency ω_h, associated to the relaxation time τ, lays just above the boson peak for both materials, shown in Fig. 6.

TABLE II. Fit parameters and magnitudes determined from MD simulation.

QR (K s^{-1})	K_0	K_∞	G_0	G_∞	$\frac{Q_T}{Q_L}$	Q_L (nm^{-1})	Q_{Lexp}	ω_h	$\omega_{\Gamma,L}$ (THz)	$\omega_{\Gamma,T}$
		(GPa)								
					$Pd_{82}Si_{18}$					
10^{13}	160	160	20	44	1.55	24.7	28.6	15	10	10
10^{12}	160	163	27	45	1.59	24.7	28.6	15	10	10
					$Zr_{50}Cu_{40}Al_{10}$					
10^{13}	104	104	20	30	1.41	25.6	26.5	11	13	10
10^{12}	105	105	20	30	1.45	25.7	26.5	11	14	10
10^{10}	103	103	21	31	1.38	25.8	26.5	9		

The frequencies $\omega_{\Gamma,(L,T)}$ of the ω^2/ω crossover, determined from Fig. 5, are also shown in Table II. A remarkable correspondence can be seen between the transverse crossover frequency $\omega_{\Gamma,T}$ and the determined relaxation frequency ω_h in $Zr_{50}Cu_{40}Al_{10}$, pointing to a link between the hardening process and the dynamics of transverse excitations. On the contrary, $\omega_h > \omega_{\Gamma,T}$ in $Pd_{82}Si_{18}$, but, as previously indicated, the behavior of high-frequency excitations is strongly affected by the presence of Einstein oscillators in this case.

V. DISCUSSION AND CONCLUSIONS

The above results confirm that there is a substantial change in the phonon propagation mode in metallic glasses in the terahertz range, connected to a strong increase on the shear modulus. The frequency of the transition appears at the end of the boson peak. The QLV model developed by Schober [7] predicts the increase of the slope in the phonon dispersion relation at a frequency related to the boson peak. Below this frequency, coupled QLV dominate the phonon spectrum and are responsible for the boson peak, while above it quasilocalized vibrations become uncoupled. The model predicts also a ω^4 dependence of the sound-speed attenuation for the low-frequency region which was insinuated here, though it could not be completely confirmed. On the whole, our results are consistent with the QLV picture, though a further structural characterization is needed to assure the validity of the QLV description.

The ability of a simple Maxwell model to describe this soft/hard transition can be interpreted in terms of the presence of a relaxation process; vibrations faster than the characteristic relaxation see a stiffer structure. The presence of elastic relaxations or nonaffine rearrangements, with characteristic times of the order of the picosecond, is a known characteristic of amorphous structures [35]. They have been estimated to create a reduction of around 10% (Bulk) and 30% (Shear) of the elastic constants with respect to the "Born terms" calculated considering only affine deformations [20,36]. In this picture, our results would indicate that the interaction of the nonaffine rearrangements with the propagating vibration modes would be not only responsible of the change in elastic constants but also responsible for the ω^2 damping behavior. This coincides with the view suggested by Baldi *et al.* [8] of a transition between glasslike modes, at low wave numbers, and crystal-like modes, at high wave numbers. The different frequency dependencies of the sound attenuation coefficients

are also the signatures of the different phonon modes, in a similar way than what was found in amorphous silica and polycrystalline quartz. If the transition between the "hard" and "soft" elastic regimes at the THz frequencies indicates an onset of glassy dynamics, this may be related to the onset of the fast secondary relaxation processes originating the high-frequency loss detected experimentally in glass susceptibility [37,38].

Not less important, our results in the macroscopic limit ($q \rightarrow 0$) solve the controversy about the behavior of the sound speed in glasses. Both the longitudinal and transverse sound speeds have constant values up to the nm length scale. In fact, the glass behaves as a continuum both in the macroscopic region and in the boson peak region. It is above the boson peak frequency when the changes in the phonon propagation mode become determinant.

Several questions still remain open. The first is why simulations using EAM offer results that differ from those performed using LJ and SS potentials. As the shear modulus is responsible for the frequency of transverse excitations, the specific description of the shear forces plays a dominant role in their behavior. Being a two-body potential, LJ systems have shear interactions that differ substantially from realistic metallic systems, and this may explain the observed differences. The second question is that anomalies of the phonon spectra of metallic glasses have been generally associated to the existence of compositional and structural inhomogeneities. However, a single relaxation frequency ω_h governs both longitudinal and transverse relations of dispersion, close to the frequency $\omega_{\Gamma,(L,T)}$, at which the phonon damping behavior also changes. This behavior, summed to the fact that no signs of any well-defined length scale were found in our simulations, prevents us to relate the transition between different phonon modes to spatial inhomogeneities. Finally, it would be very interesting to identify the quasilocalized vibrations in the molecular dynamics simulations or correlate them with some structural features in order to confirm the validity of Schober's model.

In summary, numerical simulation of the phonon spectra of metallic glasses confirms a change in the phonon regime in the terahertz range. Below this frequency range, both in the macroscopic range and in the boson peak region, the glass behaves as a continuum and the sound speed is constant. In the terahertz range the phonon dynamics is governed by a substantial increase of the shear modulus. The experimentally reported hardening of the sound speed in the nanometer range may be due to the uncoupling of quasilocalized vibrations marking the end of the boson peak. This "viscoelastic-like" transition is well described by a single relaxation frequency. The dispersion of the IXS results obtained in metallic glasses may be a consequence of different relaxation frequencies in the different amorphous structures.

ACKNOWLEDGMENTS

Work was funded by MINECO (FIS2014-54734-P) and Generalitat de Catalunya (2014SGR 581). Simulations were performed at the Barcelona Supercomputer Center, Grants No. FI-2013-1-0019 and No. QCM-2015-2-0017.

[1] H. W. Sheng, W. K. Luo, F. M. Alamgir, J. M. Bai, and E. Ma, Nature **439**, 419 (2006).
[2] Y. Zhang, C. Z. Wang, F. Zhang, M. I. Mendelev, M. J. Kramer, and K. M. Ho, Appl. Phys. Lett. **105**, 151910 (2014).
[3] T. Ichitsubo, S. Hosokawa, K. Matsuda, E. Matsubara, N. Nishiyama, S. Tsutsui, and A. Q. R. Baron, Phys. Rev. B **76**, 140201 (2007).
[4] T. Ichitsubo, W. Itaka, E. Matsubara, H. Kato, S. Biwa, S. Hosokawa, K. Matsuda, J. Saida, O. Haruyama, Y. Yokoyama, H. Uchiyama, and A. Q. R. Baron, Phys. Rev. B **81**, 172201 (2010).
[5] P. Bruna, J. Serrano, E. Pineda, M. Duarte, K. Zhao, W. Wang, and D. Crespo, Intermetallics **30**, 148 (2012).
[6] P. Bruna, G. Baldi, E. Pineda, J. Serrano, J. B. Suck, D. Crespo, and G. Monaco, J. Chem. Phys. **135**, 101101 (2011).
[7] H. Schober, J. Non-Cryst. Solids **357**, 501 (2011).
[8] G. Baldi, M. Zanatta, E. Gilioli, V. Milman, K. Refson, B. Wehinger, B. Winkler, A. Fontana, and G. Monaco, Phys. Rev. Lett. **110**, 185503 (2013).
[9] P. Lunkenheimer, L. C. Pardo, M. Köhler, and A. Loidl, Phys. Rev. E **77**, 031506 (2008).
[10] G. Monaco and S. Mossa, Proc. Natl. Acad. Sci. U.S.A. **106**, 16907 (2009).
[11] M. Li, C. Z. Wang, S. G. Hao, M. J. Kramer, and K. M. Ho, Phys. Rev. B **80**, 184201 (2009).
[12] A. Marruzzo, W. Schirmacher, A. Fratalocchi, and G. Ruocco, Sci. Rep. **3**, 1407 (2013).
[13] G. Monaco and V. M. Giordano, Proc. Nat. Acad. Sci. U.S.A. **106**, 3659 (2009).
[14] H. Mizuno, S. Mossa, and J. Barrat, Europhys. Lett. **104**, 56001 (2014).
[15] H. Mizuno, S. Mossa, and J. Barrat, Proc. Natl. Acad. Sci. U.S.A. **111**, 11949 (2014).
[16] G. Ruocco, F. Sette, R. Di Leonardo, G. Monaco, M. Sampoli, T. Scopigno, and G. Viliani, Phys. Rev. Lett. **84**, 5788 (2000).
[17] T. Voigtmann, Phys. Rev. Lett. **101**, 095701 (2008).
[18] L. Berthier and G. Tarjus, Phys. Rev. Lett. **103**, 170601 (2009).
[19] P. Derlet, R. Maaß, and J. Löffler, Eur. Phys. J. B **85**, 148 (2012).
[20] F. Leonforte, R. Boissière, A. Tanguy, J. P. Wittmer, and J. L. Barrat, Phys. Rev. B **72**, 224206 (2005).
[21] Y. H. Liu, D. Wang, K. Nakajima, W. Zhang, A. Hirata, T. Nishi, A. Inoue, and M. W. Chen, Phys. Rev. Lett. **106**, 125504 (2011).
[22] M. S. Daw and M. I. Baskes, Phys. Rev. B **29**, 6443 (1984).
[23] Y. Q. Cheng, E. Ma, and H. W. Sheng, Phys. Rev. Lett. **102**, 245501 (2009).
[24] H. Sheng, Pdsi eam potentials (2011), https://sites.google.com/site/eampotentials/home/pdsi.
[25] S. Plimpton, J. Comp. Phys. **117**, 1 (1995).
[26] T. Scopigno, J. B. Suck, R. Angelini, F. Albergamo, and G. Ruocco, Phys. Rev. Lett. **96**, 135501 (2006).
[27] Z. Zhou, C. Uher, D. Xu, W. L. Johnson, W. Gannon, and M. C. Aronson, Appl. Phys. Lett. **89**, 031924 (2006).
[28] S. Hosokawa *et al.* (ISMANAM, Paris, 2015) (unpublished).

[29] See Supplemental Material at http://link.aps.org/supplemental/10.1103/PhysRevB.94.144205 for the values of the sound speed at higher and lower quenching rates.
[30] J. Hafner, Phys. Rev. B **27**, 678 (1983).
[31] J. Hafner and M. Krajci, J. Phys.: Condens. Matter **6**, 4631 (1994).
[32] A. Matic, D. Engberg, C. Masciovecchio, and L. Börjesson, Phys. Rev. Lett. **86**, 3803 (2001).
[33] H. Shintani and H. Tanaka, Nat. Mater. **7**, 870 (2008).
[34] M. V. Vora, Glass Phys. Chem. **34**, 671 (2008).
[35] G. Knuyt, L. Deschepper, and L. Stals, J. Phys. F **16**, 1989 (1986).
[36] G. Knuyt and L. Stals, Philos. Mag. B **64**, 299 (1991).
[37] K. L. Ngai, S. Capaccioli, D. Prevosto, and L.-M. Wang, J. Phys. Chem. B **119**, 12519 (2015).
[38] Z. Wang, K. L. Ngai, W. H. Wang, and S. Capaccioli, J. Appl. Phys. **119**, 024902 (2016).